Inorganica Chimica Acta 361 (2008) 3926–3930

Contents lists available at ScienceDirect

Inorganica Chimica Acta

journal homepage: www.elsevier.com/locate/ica

Syntheses, structures and magnetic properties of iron(II) complexes with bulky tridentate ligands

Masayuki Nihei, Lingqin Han, Hirotaka Tahira, Hiroki Oshio *

Graduate School of Pure and Applied Sciences, University of Tsukuba, Tennodai 1-1-1, Tsukuba 305-8571, Japan

ARTICLE INFO

Article history:
Received 5 February 2008
Accepted 3 March 2008
Available online 8 April 2008

We dedicate this article to Professor Dante Gatteschi for his contribution to molecular magnetism.

Keywords:
Tridentate nitrogen ligand
Ferrocene
Molecular magnetism
Iron

ABSTRACT

Iron(II) complexes $[Fe^{II}(dppFc)_2](X)_2 \cdot n(solv.)$ ($\mathbf{1}(X)_2 \cdot n(solv.)$) (dppFc = 1-ferrocenyl-2-{(2,6-bis(pyrazol-yl)pyridyl)-ethylene}, $X = I_3^-$, BPh_4^-, $[Ni(mnt)_2]^-$) were prepared and their magnetic properties were studied. The central iron(II) ion in $\mathbf{1}(X)_2 \cdot n(solv.)$ was coordinated by two tridentate ligands, which have redox active ferrocenyl groups. Magnetic susceptibility measurements revealed that the central iron(II) ions in $\mathbf{1}^{2+}$ and in ferrocenes are in high- and low-spin states, respectively, in the temperature range measured.

1. Introduction

Iron(II) spin-crossover (SCO) complexes show a thermally induced spin transition between high-spin and low-spin states [1], and these have attracted research interests from view points of application to display and memory devices [2]. Spin transitions between high-spin and low-spin states associate with a large structural change, and their temperature variation of the spin transitions is strongly affected by coordination environments about iron(II) ions and crystal packing manner [3]. Iron(II) complexes with tridentate ligands such as 2,6-di(pyrazol-1-yl)pyridine (dpp) and their derivatives have been recognized as thermally induced SCO complexes [4]. We have reported an iron(II) SCO complex with ferrocenyl groups as a part of the ligand, $[Fe^{II}(dppFc)_2](BF_4)_2 \cdot 2Et_2O$ ($\mathbf{1}(BF_4)_2 \cdot 2Et_2O$) (dppFc = 1-ferrocenyl-2-{(2,6-bis(pyrazolyl)pyridyl)-ethylene} (Scheme 1)) [5]. $\mathbf{1}(BF_4)_2 \cdot 2Et_2O$ showed a single-crystal-to-single-crystal transformation induced by the release of solvent molecules, and the transformation from $\mathbf{1}(BF_4)_2 \cdot 2Et_2O$ to $\mathbf{1}(BF_4)_2 \cdot Et_2O$ changes their magnetic properties from high-spin to spin-crossover [5]. In $\mathbf{1}(BF_4)_2 \cdot 2Et_2O$, complex cations and BF_4^- anion formed a 3D network and its stable networking structure is responsible for keeping single crystallinity upon the release and adsorption of one diethyl ether molecule. Intermolecular interactions are known to affect SCO behavior. It is, therefore, expected that compounds $\mathbf{1}^{2+}$ with different counter anions have different 3D networks and show magnetic behavior different from $\mathbf{1}(BF_4)_2 \cdot 2Et_2O$. We report here the syntheses, structure and magnetic properties of iron(II) complexes $\mathbf{1}(X)_2 \cdot n(solv.)$ ($X = I_3^-$, BPh_4^-, $[Ni(mnt)_2]^-$ (mnt^{2-} = maleonitriledithiolate)).

2. Experimental

2.1. Syntheses

All the reagents were purchased and used without further purification. 1-Ferrocenyl-2-{(2,6-bis(pyrazolyl)pyridyl)-ethylene} (dppFc) and $(Bu_4N)[Ni(mnt)_2]$ (mnt = maleonitriledithiolate) were synthesized according to the literature methods [5,6].

2.1.1. $[Fe(dppFc)_2](I_3)_2$ ($1(I_3)_2$)

A mixture of $Fe(BF_4)_2 \cdot 6H_2O$ (40 mg, 0.12 mmol), dppFc (100 mg, 0.24 mmol), and L(+) ascorbic acid (small amount) in methanol (3 mL) was stirred for 30 min at room temperature. The resulted purple precipitate was filtered off and washed with methanol to give purple microcrystals of $\mathbf{1}(BF_4)_2$ (95 mg, 0.089 mmol, 74%). Diffusion of the diethyl ether to $\mathbf{1}(BF_4)_2$ (6.7 mg, 0.0062 mmol) and $(Bu_4N)I_3$ (19.0 mg, 0.030 mmol) in $MeNO_2$ (2 mL) gave purple plate crystals of $\mathbf{1}(I_3)_2$ (8.5 mg, 0.0051 mmol, 82%). *Anal.* Calc. for $C_{46}H_{38}N_{10}Fe_3I_6 \cdot 2H_2O$: C, 32.58; H, 2.50; N, 8.26. Found: C, 32.50; H, 2.23; N, 7.95%.

* Corresponding author.
E-mail address: oshio@chem.tsukuba.ac.jp (H. Oshio).

0020-1693/$ - see front matter © 2008 Elsevier B.V. All rights reserved.
doi:10.1016/j.ica.2008.03.118

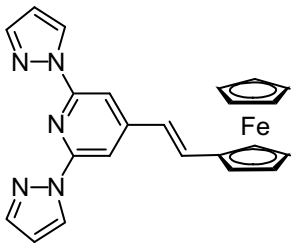

Scheme 1. Molecular structure of dppFc.

*2.1.2. [Fe(dppFc)$_2$](BPh$_4$)$_2$ · Et$_2$O · 3(MeNO$_2$) (**1**(BPh$_4$)$_2$ · Et$_2$O · 3(MeNO$_2$))*

Diffusion of the diethyl ether to **1**$(BF_4)_2$ (6.7 mg, 0.0062 mmol) and $(Bu_4N)BPh_4$ (19 mg, 0.034 mmol) in $MeNO_2$ (2 mL) gave purple plate crystals of **1**$(BPh_4)_2 \cdot Et_2O \cdot 3(MeNO_2)$ (8.5 mg, 0.0047 mmol, 76%). *Anal.* Calc. for $C_{94}H_{78}N_{10}Fe_3B_2 \cdot 2(H_2O)$: C, 71.78; H, 5.25; N, 8.90. Found (dried sample): C, 71.70; H, 5.12; N, 8.65%.

*2.1.3. [Fe(dppFc)$_2$][Ni(mnt)$_2$]$_2$ (**1**[Ni(mnt)$_2$]$_2$)*

Diffusion of the diethyl ether to **1**$(BF_4)_2$ (11.2 mg, 0.010 mmol) and $(Bu_4N)[Ni(mnt)_2]$ (21.6 mg, 0.037 mmol) in $MeNO_2$ (3 mL) gave purple plate crystals of **1**$[Ni(mnt)_2]_2$ (3.7 mg, 0.0023 mmol, 23%). *Anal.* Calc. for $C_{62}H_{38}N_{18}Fe_3Ni_2S_8$: C, 47.23; H, 2.43; N, 15.99. Found: C, 47.02; H, 2.52; N, 15.87%.

2.2. X-ray crystallography

Each crystal of **1**$(X)_2$·(solv.) was mounted on a glass capillary, and the X-ray diffraction data were collected at −73 °C (Bruker SMART APEX diffractometer coupled with a CCD area detector with graphite monochromated Mo Kα (λ = 0.71073 Å) radiation). The structures were solved by direct methods and expanded by using Fourier techniques using SHELXTL program. Empirical absorption corrections were carried out by SADABS (G.M. Sheldrick, 1994). In the structure analyses, non-hydrogen atoms were refined with anisotropic thermal parameters. Hydrogen atoms were included in the calculated positions and refined with isotropic thermal parameters riding on those of the parent atoms. Crystal data and coordination bond lengths are summarized in Tables 1 and 2, respectively.

Table 2
Coordination bond lengths (Å) of complexes

	1$(I_3)_2$	**1**$(BPh_4)_2 \cdot Et_2O \cdot 3(MeNO_2)$	**1**$[Ni(mnt)_2]_2$
Fe–N1	2.135(9)	2.141(4)	2.121(4)
Fe–N2	2.192(10)	2.180(3)	2.174(5)
Fe–N4	2.204(10)	2.205(3)	2.177(5)
Fe–N6	2.126(9)	2.131(4)	
Fe–N7	2.193(9)	2.166(4)	
Fe–N9	2.170(10)	2.163(4)	

2.3. Magnetic measurements

Magnetic susceptibility data of **1**$(X)_2$·(solv.) were collected by using a Quantum Design MPMS-XL SQUID magnetometer in the temperature range from 5 to 300 K.

3. Results and discussion

3.1. Descriptions of crystal structures: [Fe(dppFc)$_2$](I$_3$)$_2$ (**1**(I$_3$)$_2$)

1$(I_3)_2$ crystallized in triclinic space group $P\bar{1}$, and the asymmetric unit is composed of one complex cation and two triiodide ions. An ortep diagram of a cation is shown in Fig. 1. Charge consideration of component molecules suggests that the complex cation has a 2+ charge and the ferrocenyl groups contain low-spin iron(II) ions. The central iron(II) ion is coordinated by six nitrogen atoms from two tridentate dppFc, giving significantly distorted octahedral coordination geometry. Coordination bond lengths of Fe–$N1_{pyridyl}$ and Fe–$N6_{pyridyl}$ are 2.135(9) Å and 2.126(9) Å, respectively, while Fe–$N_{pyrazole}$ (Fe–N2, N4, N7 and N9) are in the range of 1.958(6)–1.983(7) Å. The coordination bond lengths are the characteristic of high-spin iron(II) ions [1]. Distortion of the coordination sphere from ideal octahedron relates ligand field strength on iron ions,

Table 1
Crystallographic data for complexes

	1$(I_3)_2$	**1**$(BPh_4)_2 \cdot Et_2O \cdot 3(MeNO_2)$	**1**$[Ni(mnt)_2]_2$
Formula	$C_{46}H_{38}Fe_3I_6N_{10}$	$C_{101}H_{85}B_2Fe_3N_{13}O_7$	$C_{62}H_{38}Fe_3N_{18}Ni_2S_8$
Formula weight (g mol^{-1})	1659.81	1782.03	1576.56
Temperature (K)	200	200	200
Wavelength (Å)	0.71073	0.71073	0.71073
Crystal system	triclinic	triclinic	monoclinic
Space group	$P\bar{1}$	$P\bar{1}$	$C2/c$
a (Å)	12.0136(19)	16.155(7)	28.35(3)
b (Å)	14.012(2)	16.821(7)	9.615(9)
c (Å)	17.268(3)	17.883(8)	26.64(2)
α (°)	82.214(3)	77.024(9)	
β (°)	78.702(3)	81.620(9)	119.090(12)
γ (°)	71.314(3)	71.218(9)	
V (Å^3)	2692.0(7)	4469(3)	6345(10)
Z	2	2	4
d_{calc} (Mg m^{-3})	2.048	1.332	1.650
μ (mm^{-1})	4.279	0.545	1.573
θ Range for data collection (°)	1.21–23.28	1.17–25.51	2.27–26.04
Index ranges	$-13 \leqslant h \leqslant 13$, $-15 \leqslant k \leqslant 15$, $-19 \leqslant l \leqslant 18$	$-17 \leqslant h \leqslant 19$, $-17 \leqslant k \leqslant 20$, $-21 \leqslant l \leqslant 21$	$-31 \leqslant h \leqslant 34$, $-11 \leqslant k \leqslant 11$, $-32 \leqslant l \leqslant 20$
Reflections collected	12229	23995	14007
Independent reflections (R_{int})	7675 (0.0230)	16090 (0.0312)	5577 (0.0605)
Maximum and minimum transmission	0.6742 and 0.4815	0.9475 and 0.8988	0.8585 and 0.7438
Data/restraints/parameters	7675/0/586	16090/0/1159	5577/0/420
Goodness-of-fit on F^2	1.071	1.008	1.010
Final R indices [$I > 2\sigma(I)$]	R_1 = 0.0537, wR_2 = 0.1866	R_1 = 0.0683, wR_2 = 0.1706	R_1 = 0.0642, wR_2 = 0.1384

$R_1 = \sum||F_o| - |F_c||/\sum|F_o|$. $wR_2 = [\sum[w(F_o^2 - F_c^2)^2]/\sum[w(F_o^2)^2]]^{0.5}$.